

1 Large scale excavation of outer shelf sediments by bottom currents during 2 the Late Miocene in the SE Atlantic

3 Andrew Hopkins^{1, 2} and Joe Cartwright³

4 Email: andrew.hopkins@ucl.ac.uk

5 Abstract

6 An unusual erosional surface has been identified on seismic data from the outer shelf on the northern
7 Namibian margin. The undulating surface defines a depression extending for 1,300 km² from which fine-
8 grained Miocene sediments have been excavated to a depth of up to 160 m. The depression has a kidney-
9 shaped planform, with three deep pits marking its basinward extent. It is an entirely closed feature, with no
10 evident channels feeding in or leading out. Subsequent sedimentation has completely filled in the depression
11 with the earliest infilling units exhibiting unusual depositional geometries. Well correlation yields a date of
12 9.9 ± 1.0 Ma for the erosional surface. No analogous features are known, but of all the possible causal
13 mechanisms, it is considered most likely that the erosional depression was created by the extraordinary
14 action of eddying bottom currents. These were probably associated with the well-documented Late Miocene
15 onset of intensification of the Benguela Upwelling System, and were possibly directed by a small local
16 variation in sea bed relief.

17 Funding

18 AH received a one off Grant-in Aid from the American Association for Petroleum Geology for work which
19 included this study.

20 Conflicts of interest/Competing interests (include appropriate disclosures)

21 Not applicable.

22 Availability of data and material

¹ School of Earth and Ocean Sciences, Cardiff University, CF10 3AT, UK.

² Department of Science and Technology Studies, University College London, WC1E 6BT, UK. ORCID: 0000-0003-1646-0549

³ Department of Earth Sciences, University of Oxford, OX1 3AN, UK. ORCID: 0000-0003-4198-9719

23 Seismic and well data are owned by Namcor, the National Petroleum Corporation of Namibia; DSDP and ODP
24 data are open access

25 **Code availability**

26 Not applicable.

27 **Consent to participate (include appropriate statements)**

28 Not applicable.

29 **Consent for publication**

30 Namcor - pending

31 **1. Introduction**

32 The growing body of literature examining the products and processes attributable to the action of marine
33 bottom currents is dominated by examples from continental slopes and from basin floors. (e.g. Rebesco et al
34 2014). Far fewer cases have been reported from continental shelf environments, a bias that can be explained
35 by the fact that the global thermohaline system tends to operate at depths below several hundred metres.
36 The relatively uncommon sediment drifts and erosional features that do occur on continental shelves are
37 generally attributed to more localised current regimes. They can however be significant in scale (e.g.
38 Fulthorpe and Carter 1991; Verdicchio and Trincardi 2008) and they have possible implications for aspects of
39 petroleum geology. For example, they may be important for understanding the impact of shallow-water
40 bottom currents on shelf anoxia, on the reworking and distribution of shelf reservoirs and on the delivery of
41 shelfal sands to deeper water environments.

42 In this paper we discuss the interpretation of a 2D seismic dataset from the northern Namibian continental
43 margin (Figs. 1 and 2). Within the dataset, we have identified a highly unusual morphological depression
44 with an areal extent of 1,300 km² and up to 160 m of relief (Fig 3). This large depression is hosted in
45 sediments deposited on the palaeo-shelf during the Neogene. It is therefore presumed to have formed
46 under shallow bathymetric conditions. However, unlike all other major erosional features that are known to
47 form in shelf environments such as incised valleys or submarine canyons, this feature has a closed perimeter,

48 i.e. it does not open into the deeper water but is entirely enclosed on all its lateral margins. Superficially it
49 thus resembles a large crater, and we consider a range of possible known crater-forming mechanism such as
50 caldera collapse (e.g. Branney 1995), bolide impact (e.g. Stewart 2003) and focused fluid expulsion (e.g.
51 Cartwright and Santamarina 2015). Also, by analysing the external morphology, truncation geometry and
52 disposition of the sedimentary infill, we consider the possibility that this feature was caused by intensive
53 vertical eddying in shelfal water depths off the coast of Namibia, during the Late Miocene. Contemporary
54 eddy systems are well known from this part of the South Atlantic (e.g. Clement and Gordon 1995; Penduff et
55 al 2001), and we draw on modern analogues in weighing up this possible explanation. If correct, this would
56 be the first such description of large scale erosion by a major oceanic eddy system on a continental shelf in
57 the stratigraphic record, with concomitant implications for the interpretation of shelf systems in a wider
58 sense.

59 2. Regional geological setting

60 2.1 Modern physiographic setting

61 The study area is located about 60 km offshore at the northern end of the present-day Cape Basin (Fig. 1). It
62 covers part of the southern flank of the aseismic Walvis Ridge, which separates the Cape Basin from the
63 Angola Basin to the north, and which runs from its coastal abutment for 2,500 km towards the Mid Atlantic
64 Ridge. It forms a barrier to northward and southward flow below a water depth of about 3,000m (Shannon
65 1985) and thus exerts a major influence on deep circulation in the southeast Atlantic. The present-day
66 continental shelf along this part of the Namibian margin is unusually wide at about 40 km, with a relatively
67 broad and upwardly convex shelf-slope break. The water depth at the shelf break as measured on seismic
68 data ranges from 350 to 400 m, which is unusually deep by global norms (Van Andel and Calvert 1971).

69 2.2 Geological evolution

70 Recent studies place the onset of sea-floor spreading in the southernmost Atlantic within the Valanginian
71 (Perez-Diaz and Eagles 2014: 138 Ma; Hall et al. 2018: 135 Ma). Plate reconstructions point to a northward
72 opening of the South Atlantic, such that break up took place sequentially across a series of segment

73 boundaries aligned perpendicular to the margin (Heine et al. 2013). The part of the margin immediately
74 south of the Walvis Ridge (known as the Walvis Basin, e.g. Light et al. 1993), underwent an initial period of
75 extensional faulting in the late Albian. Subsequently, a predominantly clastic depositional system became
76 established, infilling the rifted topography, and superseding a succession of pre-rift platform carbonates
77 (Holtar and Forsberg 2000). At the northern end of the Walvis Basin a major submarine volcanic centre, the
78 Phoenix High (*P* in Fig. 1), was emplaced on the south side of the Walvis Ridge in Cenomanian to Turonian
79 times (Corner et al. 2002) and was subsequently buried by later sediment. Drilling results indicate that the
80 post-rift succession is mud-dominated, and is punctuated only rarely by sandy turbiditic flows (Holtar and
81 Forsberg 2000). The Angolan margin to the north of the Walvis Ridge experienced major uplift and rotation
82 during the Miocene (Jackson et al. 2005). However, there is no evidence of significant tectonic or gravity-
83 driven deformation at any time during the Neogene, the main interval of interest for this study, in the basins
84 to the south.

85 **2.3 Neogene stratigraphy and palaeoceanography**

86 ODP and DSDP wells (from Sites 352 and 1081 respectively) provide valuable information on
87 lithostratigraphy (Diester Haass et al. 1990; Pufahl et al. 1998). The Neogene sedimentary succession
88 comprises almost entirely hemipelagic muds, clays and calcareous oozes, with a significant biogenic
89 component, reflecting the paucity of land-derived material due to the aridity of the adjacent onshore areas
90 (Aizawa et al. 2000). The biogenic components demonstrate the high productivity of the margin, which is
91 one of the world's most prolific upwelling systems. Evidence from palaeoproductivity proxies, together with
92 other studies of regional oceanography and onshore geology, indicates that cold water has been upwelling
93 along the Namibian margin since ca. 10 Ma (Siesser 1980; Rommerskirchen et al. 2011). Upwelling started in
94 response to the intensification of the Benguela Upwelling System (BUS, Fig. 1), which had been active in a
95 weak form since ca. 14 Ma (Diester Haass et al. 1990). Onshore, in response to the strengthening BUS, the
96 existing semi-arid conditions were intensified leading to the interior becoming hyper-arid. Landscapes were
97 stabilised with the development of pedogenic calcretes (Ward and Corbett 1990), further limiting erosion.

The two main near-shore components of the BUS are the cold, northward flowing Benguela Current (BC), and the Angola Current (AC), which brings warm, tropical water southward (Fig.1). The coastal branch of the BC, the Benguela Coastal Current (BCC) and the AC converge at the Angola-Benguela Front (ABF), a line roughly perpendicular to the margin, to create a zone of strong current activity and eddying (Lass et al. 2000). The ABF has moved northwards and southwards along the Angolan-Namibian margin during its existence in response to changes in hydrography and wind stress (Jansen et al. 1996).

3. Database and methods

3.1 Seismic data

The study is based on the interpretation of 7,900 line kilometres of time-migrated seismic reflection profiles (Fig. 2). These were acquired during petroleum exploration campaigns in the 1990s (Holtar and Forsberg 2000), and the study area, which is bounded by the red outline on Fig. 2, corresponds to Licence Block 1911. This high-resolution multichannel dataset is arranged orthogonally with lines spaced between 2 and 8 km apart. Reflections within the interval spanning the erosion surface and its infill have resolution limits of ca. 15 m vertically and ca. 25 m laterally. These limits are based on a dominant frequency of 60 Hz and assume average P-wave interval velocity of 1,600 m/s (for poorly consolidated shelf sediments), and are calculated using standard formulations (Sheriff 1977). Data quality is generally excellent with a high signal-to-noise ratio. The zone of interest is too shallow to be affected by sea-bed multiples, though some short period reverberations are evident (see Section 4.2).

Two deep oil exploration boreholes (1911/10-1 and 1911/15-1) and ODP well 1081A are situated within 40 km of the basinward side of the feature (Figs. 2 and 3). All three intersect the seismic grid and provide valuable stratigraphic calibration. Standard seismic-stratigraphic interpretation techniques were used to identify and correlate prominent stratigraphic surfaces, including the major erosional surface that forms the focus of this study (Mitchum et al. 1977; Brown and Fisher 1977). Geoframe and IHS Markit Kingdom software were used for digital seismic interpretation. Individual horizons were, however, picked manually following accepted principles rather than by automatic tracking correlation (e.g. Ashcroft 2011).

4. Results

4.1 Seismic stratigraphy

The seismic stratigraphy of the Walvis Basin has been divided by previous authors into major “geometrically confined” tectono-stratigraphic units (Holtar and Forsberg 2000; see also e.g. Light et al. 1993). The post-rift units highlighted in Figure 4 (see Fig. 2 for location) broadly correspond to the “W” prefixed sub-divisions of Holtar and Forsberg (2000) as follows: Late Albian to Maastrichtian: W3 to W5; Palaeocene and Eocene: W6-1 to W6-4; Oligocene to Early Miocene: W6-5; Early to Late Miocene: W6-5 to W6-6; Late Miocene to Recent: W7.

All of the post-rift units consist of mainly fine-grained sediments. The seismic configurations of the pre-Early Miocene units are dominantly progradational/aggradational. The Early to Late Miocene unit however is characterised by a much more aggradational stacking configuration on both the shelf and the slope (Aizawa et al. 2000). The youngest, Late Miocene to Recent seismic-stratigraphic unit onlaps against the outer shelf break and is notably absent (or considerably condensed) on the modern shelf. Our main focus is on the Early to Late Miocene unit on the shelf, which is characterised by laterally continuous reflections that provide excellent constraints for regional chrono-stratigraphic correlation (Fig. 4).

4.2 Seismic interpretation of the erosion surface

The erosional nature of the surface is evident from the systematic truncation of underlying stratal reflections in the centre of the study area. Using standard interpretation techniques (Vail et al. 1977; Emery and Myers 1996), the highly undulating erosion surface can be interpreted on 17 dip lines and 7 strike lines as a prominent seismic reflection generally occurring within 150 ms (TWTT or ca.120 m) of the present day sea-floor. The depression formed by the erosion surface corresponds to the envelope of truncated reflection terminations (Figs. 5 and 6). Truncation geometries are pronounced, often with relatively large angles of up to 12 degrees (e.g. Fig. 6d), which are classically typical of erosional processes that involve localised excavation of the substrate or down-cutting (Brown and Fisher 1977; Emery and Myers 1996). The infilling

147 sediments exhibit onlapping and downlapping reflection configurations at the margins of the erosional
148 depression (Figs. 5 and 6).

149 The erosion surface occurs in continuous segments and is readily identifiable, especially where truncation is
150 angular (see examples of erosional truncation in Figs. 5 and 6). Generally the surface produces a high
151 amplitude positive or 'hard' reflection signifying an increase in acoustic impedance. Amplitude, phase and
152 polarity do however vary somewhat as the acoustic properties of the lithologies juxtaposed above and below
153 the erosion surface vary. The unambiguous truncation geometry of the reflection is however occasionally
154 obscured by short period reverberations (follow cycles, e.g. Fig. 5a), and by the low frequency water bottom
155 reflection. The spacing of the dip lines is considered adequate to avoid significant spatial aliasing (Emery and
156 Myers 1996).

157 Laterally, the erosion surface passes into a concordant package of reflections as a correlative conformity
158 (*sensu lato*, e.g. Fig. 6d). However, some of the correlative reflections do not quite tie consistently at line
159 intersections which may indicate a degree of diachroneity. Alternatively, the minor mistie problem may
160 simply be due to the intrinsic limit of vertical resolvability at the lateral margin of the erosion surface.

161 **4.3 Morphology of the erosion surface**

162 The erosion surface has a planform that is roughly kidney shaped, measuring approximately 40 by 50 km
163 with a slight elongation orthogonal to the coastline, i.e. in a NE-SW direction (Fig. 3). Importantly for any
164 consideration of the origins of this erosional feature, the mapped positions of its margins reveal it to be
165 entirely enclosed. That is, it does not open out anywhere into another erosional feature, but is completely
166 surrounded by conformable reflection configurations. No channels feeding into the erosional feature from
167 the palaeo-coastline are evident (Fig. 3).

168 A 3D visualisation of the erosional feature constructed from the gridded interpretation (Fig7) shows the
169 depression wrapping around the southern and south-eastern sides of a low relief topographic mound (the
170 high axis in Fig 3). This is the remnant expression at the sea floor of the buried Late Cretaceous Phoenix High
171 volcanic centre ("P" in Figs. 1 and 8; see also Fig 14 in Holtar and Forsberg 2000).

172 The morphology of the erosion surface is illustrated by two representative seismic profiles (Fig. 5a and b). On
173 dip profiles, the surface forms a series of undulating, quasi sinusoidal highs and lows, with the relief on the
174 surface generally increasing basinward (Fig. 5b). The irregular relief is also evident on strike orientations,
175 though the profile is more asymmetrical, with the slope of the excavated surface being markedly more
176 gentle to the north-west than on the south-eastern side (Fig. 5a).

177 Internally, the depression consists of three curved, sub-parallel troughs with two intervening ridges (Figs. 3
178 and 7). The outermost of these troughs defines the eastern boundary of the depression and curves in strike
179 through nearly 90°, from NW-SE inshore, to SW-NE at the basinward margin. The outer edge of the
180 depression has an angular, clearly defined lip on seismic profiles, with no evidence of levees or marginal
181 build-ups (Figs. 5 and 6). The two inner troughs are shorter and much less curved, and are encompassed by
182 the arc of the long outer trough. All three troughs become less well defined towards the north-western end
183 of the depression, which tapers to a point. The three troughs merge here and level off into a broad, relatively
184 flat area (Figs. 3 and 7).

185 On the basinward side of the erosional depression, each of the three troughs shallows before plunging down
186 into a deep, terminal pit (Figs. 3 and 7). These three pits (A, B and C on Fig. 6) are perhaps the most striking
187 features of the entire erosional depression, and appear to represent loci of maximum down-cutting. There is
188 no common datum (base level) for the depth of erosion either beneath the modern seabed or beneath a
189 datum interpolated from the marginal correlative conformities surrounding the feature. There is therefore
190 no geometrical indication that the depths of the deepest portions of the erosion surface relate to any form
191 of regional base level under any definition of that term (e.g. Schumm 1993; Catuneanu 2003).

192 The three pits are all broadly elliptical in map view. Each forms a fully enclosed low of the order of 8 km in
193 length and 3-4 km in width, with an erosional relief of 100-160 m. All three are relatively symmetrical in their
194 short axis orientation (Fig. 6a), though each has an asymmetric longitudinal section (Figs. 6b, c and d), with
195 the steeper dip occurring on the basinward side. The steepest slope associated with the entire erosional
196 depression occurs on the south-west side of pit C, which dips at approximately 12° to the northwest (Fig. 6d)

197 Each of the elliptical pits is marked by a lip that defines the basinward limit of each trough (Figs. 6 and 7b).
198 They step progressively basinward by several kilometres relative to strike from southeast to northwest (Figs.
199 3 and 7b), though all three pits terminate on the upper palaeo-slope as judged by their positions relative to
200 palaeo-slope breaks on clinoform surfaces (see Section 4.5). There is no evidence that the process that
201 eroded the depression was active basinward on the surface of the palaeo-slope, which is undisturbed at a
202 seismic scale, and exhibits uniformly concordant reflection geometries.

203 **4.4 Subcrop relationships**

204 The erosion surface appears to have cut downwards into the pre-existing strata at random. That is, the
205 erosive process does not appear to have exploited any inhomogeneity or weakness in the underlying
206 stratigraphy or structure. The stratal configurations of the eroded units are parallel, conformable and sub-
207 horizontal consistent with their interpretation as former shelf deposits (Figs. 5 and 6).

208 **4.5 Palaeo-water depth**

209 The transitional form of the shelf-slope system, with no clear clinoform breakpoints (Fig. 4), makes it difficult
210 to determine palaeo-water depths. This is consistent with the conclusion that terrigenous input has been
211 severely limited throughout much of the Neogene (Pufahl et al. 1998; Aizawa et al. 2000).

212 At several points along the margin, small shelf delta systems have been preserved at the present day sea
213 floor, and these provide the means to estimate palaeo-sea level (Fig. 9). The topsets present at the sea floor
214 currently lie in about 130 m of water but would have been at or very close to sea level at the time of
215 deposition. Assuming that present day sea level includes a post-glacial rise of 120 m since the Pleistocene
216 (Gornitz 2009), the net relative sea level rise is ca. 10 m. The topsets of the shelf delta system include the
217 extrapolation of the reflection forming the correlative conformity as interpreted on the south side of the
218 erosional feature which can therefore be regarded as a time-equivalent surface. If depths to the uneroded
219 margins of the depression are approximately 340 m at the present day, then water depths at the onset of
220 erosion were about 330 m. The present-day topset surface is approximately horizontal, so it is assumed that
221 there has been negligible basinward rotation and no appreciable along-strike tilting since the time that this

major erosional episode took place. Differences in compaction along the dip profile can also reasonably be assumed to be negligible, and this palaeo-water depth estimate of 330 m can therefore be taken as a valid approximation.

4.6 Sedimentary infill – reflection configuration

The sediments infilling the eroded depression can be subdivided into two informal seismic stratigraphic units (M1 and M2), based on their distinctive seismic facies and reflection configurations (Figs. 5 and 6).

4.6.1 Unit M1

The lower unit comprises reflections that exhibit variable internal configurations and relationships to the underlying erosion surface. These configurations include onlap, drape and bi-directional downlap (Figs. 5 and 6). Reflection patterns include both parallel and divergent relationships. Most notably however, reflections in the lower unit downlap the erosion surface and prograde towards the eastern and south-eastern margins of the excavation (Fig. 5b). Downlap is particularly evident against the relatively steep sides on the outer curve of the outer trough, where the direction of progradation and downlap rotates so that it remains approximately perpendicular to the margin of the depression (see arrows in Fig. 7b). In the three elliptical pits (A, B and C of Fig. 6) however, where downlap occurs, the direction is exclusively basinward (Fig. 6b, c and d).

A strike profile across the three elliptical pits (Fig. 6a) illustrates some of the variety of reflection configurations in the lower unit. The lowermost reflections in pit A lie sub-parallel to the underlying erosion surface, and onlap or gently downlap the sides. Overlying, low amplitude reflections are mainly parallel and sub-horizontal, but with indications of divergence on the south side. In pit B, the lowermost reflections are sub-horizontal and parallel. The subsequent two or three cycles however, display bi-directional downlap. On the south flank of pit C, infilling reflections lie in a prograding, sigmoid configuration. This pattern is reminiscent of the lateral accretion that commonly occurs in submarine channel environments (Wonham et al. 2000; Abreu et al. 2003), suggesting that a similar process of axial flow that shifts progressively laterally

246 may have been operative during erosion and deposition. Overlying strata are represented by sub-horizontal
247 reflections indicating the change to a more aggradational style of deposition.

248 Unit M1 reaches a maximum thickness of up to 130 m in the elliptical pits. In the main part of the erosional
249 depression, it thickens to the southeast, towards the outer curved margin (Fig. 5a). The surface marking the
250 top of the lower unit just fails to cover all of the more prominent highs within the depression, and dips
251 gently basinward (Figs. 5 and 6).

252 *4.6.2 Unit M2*

253 Unit M2, seen overlying the green horizon in Figs. 5 and 6, is characterised by sub-horizontal, parallel
254 reflections, which are generally more continuous and have stronger amplitudes than those of the lower unit.
255 Reflections in this unit tend to be obscured by low amplitude multiples from the sea floor. Its thickness is
256 greatest over the central parts of the erosional feature, reaching about 70 m, thinning to below seismic
257 resolution around the margins.

258 The present seafloor exhibits no vestiges of the earlier episode of erosion, the feature having been
259 completely filled by the two units described, and by subsequent pelagic/hemipelagic deposition. The
260 Phoenix High however, has a continuing low relief expression at the seafloor today (Fig. 8 and see structural
261 high axis in Fig. 2).

262 **4.7 Timing of the erosional episode**

263 The erosion surface was dated by tying the correlative conformity to the most reliably dated nearby well. Of
264 the three wells in the study area, only ODP 1081A (Pufahl et al. 1998) was able to provide viable constraints
265 on age dating from biostratigraphy (Fig. 10). This borehole reached its total drilled depth 38 ms or
266 approximately 35 m⁴ above the correlative conformity surface, so extrapolation using average sedimentation

⁴ An interval velocity of 1,850 m/s was derived from check shots in the exploration wells 1911/10-1 and 1911/15-1 for Miocene sediments on the continental slope, giving a depth interval of 35 m. This interval velocity has been used in preference to the unrealistic value of 1,500 m/s which Wefer et al (1998) assumed for the entire section between the seafloor and the bottom of the hole.

267 rates was required to derive a probable age for the correlative conformity, and hence to enable the end of
268 the hiatus corresponding to the erosional episode to be bracketed.

269 Based on the oldest identified calcareous nannofossil datum (NN10), the bottom-hole date in ODP 1081A is
270 estimated at 9.0 ± 0.2 Ma (Wefer et al. 1998). Assuming constant sedimentation rates throughout the Late
271 Miocene and Early Pliocene of 4 cm/k.y. (Wefer et al. 1998) and extrapolating this rate linearly backwards,
272 the time represented by the interval of 35 m below the borehole is approximately 875,000 years. Hence the
273 erosion surface can be assigned an age of 9.9 ± 0.2 Ma using this method. The error of ± 0.2 Ma (Wefer et al.
274 1998) does not however take account of possible well-to-seismic tying errors or of potential time-to-depth
275 conversion errors. The aggregate of all these factors therefore leads to a best estimate for the minimum age
276 of the erosion surface of 9.9 ± 1.0 Ma (i.e. Late Miocene). The eroded strata are assumed to have been
277 pelagic and hemipelagic shales and mudstones of Miocene age (Stow 1987).

278 5. Discussion

279 An explanation of the processes by which a large volume of the Late Miocene outer shelf came to be
280 excavated and re-filled must be able to account for the following key observations:

- 281 1. The external asymmetric 'kidney-shaped' morphology of the excavated zone with its entirely closed
282 perimeter.
- 283 2. The proximity to the remnant of the Phoenix High, and confinement of the depression to the outer
284 continental shelf.
- 285 3. The internal structure including the three sub-parallel troughs each ending in a deep elliptical pit, the
286 inwardly dipping outer margins, and the pronounced basinward curve.
- 287 4. The gross basinward plunge of the depression with a lack of any systematic base level of erosion.
- 288 5. The timing of the concurrent episodes of erosion and infill during the Late Miocene.

289 We considered a range of mechanisms to account for the erosional excavation of this large depression
290 offshore Namibia, including collapse by withdrawal or removal of material from below, slumping, and
291 current driven erosion. The removal of underlying material by dissolution or withdrawal can cause gravity-

292 driven collapse creating a surface depression (Bertoni and Cartwright 2006; McDonnell et al. 2007). This
293 mechanism was considered because it is well known to be capable of forming a surface depression above
294 the zone of underlying collapse that is characterised by an enclosed perimeter (Branney 1995; Bertoni and
295 Cartwright 2006). It can be discounted here however, because the reflections beneath the depression are
296 undisturbed and there are no indications of the concentric faulting or down-bending that might be expected
297 in response to collapse (Bertoni and Cartwright 2006). Furthermore, the absence of halite in the sediments
298 precludes the possibility of collapse due to salt dissolution.

299 We also rejected the possibility that the depression is a slump scar. There is no evidence of any remnant
300 remobilised material with a characteristic chaotic seismic facies deposited directly on the erosion surface
301 (Frey Martinez et al. 2005; Bull et al. 2009). It is also difficult to see why a slump scar would exhibit the
302 geometry of an enclosed perimeter with inward dipping margins. Submarine slope failure surfaces invariably
303 plunge in a downslope direction, or ramp upwards through pre-failure stratigraphy at the toe region (Frey
304 Martinez et al. 2005; Masson et al. 2010), neither of which is seen here. The sense of asymmetry in the long
305 axis direction is also the opposite of what is commonly seen in slumps or rotational failures. The steepest
306 surfaces in the erosional depression lie closest to the continental slope, but face away from it, rather than
307 towards the downslope direction as would be the norm. There is also no trace of any remobilised material
308 having been transported downslope from the depression to be incorporated in the age equivalent slope
309 sediments as a mass transport complex.

310 The erosional depression is located close to the present-day outflow of the ephemeral Hoanib River (Fig. 1),
311 so we considered the possibility that the feature was formed during a relative sea level lowstand as an
312 incised valley (Posamentier 2001). However, from the palaeo-water depth reconstruction of ca. 330 m, a
313 significant fall in relative sea level would have been required to initiate and complete the incision, and there
314 is no evidence of such a dramatic relative sea level fall along this part of the Namibian continental margin
315 during the Miocene (Siesser and Dingle 1981; Aizawa et al. 2000). Even more of a problem with this incised
316 valley model, is the lack of any channel system or canyon extending basinward from the outlet of the
317 erosional depression, which is invariably observed associated with incised valleys cut into shelf sequences

318 elsewhere (Posamentier 2001; Bertoni and Cartwright 2006). The excavation as an incised valley
319 fundamentally fails to explain the enclosed perimeter, the inward dipping margins of the erosion surface,
320 and the lack of any systematic erosional base level datum. For these reasons we reject this explanation. The
321 only valleys that are known to exhibit U-shaped thalweg profiles are tunnel valleys, but since these only
322 occur as a result of sub-glacial meltwater flow (Huuse and Lykke-Andersen 2000) and the nearest glaciated
323 area at this time was in Antarctica, this possibility can also be discounted.

324 **5.1 Bottom current activity**

325 There are several lines of evidence pointing to the erosional depression having been formed as the result of
326 the action of bottom currents:

- 327 1. The apparent current entry point for the depression is aligned parallel to the margin;
- 328 2. The orientation of many of the downlapping configurations of the reflections defining the internal fill
329 also indicate a current orientation parallel to the margin;
- 330 3. Some of the reflection configurations within the infilling succession are diagnostic of contourites.

331 The erosive action of bottom currents on the continental slope of the Cape Basin was first recognised by Van
332 Andel and Calvert (1971). More recently, Late Miocene slump scars observed on seismic data from the
333 continental slope in the south of the Cape Basin have been attributed to the interaction of slope instabilities
334 with bottom currents associated with the onset of upwelling (Weigelt and Uezelmann-Neben 2004). Further
335 afield, a notable series of present-day km scale “erosive sub-circular depressions” has been reported from a
336 middle slope setting in the Gulf of Cadiz with a proposed origin partly attributable to eddying within the
337 Mediterranean Outflow Water (Garcia et al. 2016).

338 By contrast, examples of bottom current erosion impinging on the outermost shelf system, where slope
339 instability is less likely to contribute to mass movements, are comparatively rare (e.g. Fulthorpe and Carter
340 1991; Verdicchio and Trincardi 2008). On the KwaZulu-Natal continental shelf, Green (2009) has documented
341 the present-day role of the coast-parallel Agulhas Current in the redistribution of sediment and in relatively
342 minor erosive activity. However, nothing comparable to the excavation geometry described in this Namibian

343 example has previously been suggested to be linked to bottom current erosional processes. Does this imply
344 that exceptional factors were in operation during the creation of the feature? These factors must certainly
345 include the generation of sufficient current power to erode the substrate down to 300 m below the seabed.
346 They must also allow for the organisation of these currents on a sufficiently long time scale in a stable
347 position on the shelf to focus this erosional activity at the site of the excavation.

348 On the question of why this feature is located specifically where it is along the margin, two points can be
349 considered. Firstly, the flow focusing effect of sea floor topography, and secondly the timing of the
350 intensification of upwelling in the Benguela region, with the consequences for palaeo-circulation implied by
351 that event. It is well known that current pathways can be topographically steered, even by very small-scale
352 sea floor features (Gille et al. 2004). In order to conserve momentum, a flow may have to increase or
353 decrease velocity in order to negotiate a topographic change. Variations in shear velocity, and hence in bed
354 shear stress can therefore occur where fluid flow is constricted or caused to expand by changes in the
355 topography of the sea bottom (e.g. Leeder 1999). It is conceivable therefore that the 'gap' between the
356 positive topography of the Phoenix High and the shoaling of water depth towards the coast may have acted
357 as a constriction to a southward flowing bottom current. Turbulent eddies may then have been generated by
358 the intensification of flow in the unusually large water depths of the outer shelf. This induced vorticity may
359 then have been responsible for the erosional morphology as a kidney-shaped depression scour. The
360 apparent direction of overall flow suggests that the southward flowing Angola Current was instrumental in
361 the erosive process and that the ABF was situated further south than is shown in Fig. 1.

362 Following the above argument, we suggest that the detail of the erosional morphology of the three sub-
363 parallel, curved troughs with three terminal deep troughs is due to the presence of instabilities within the
364 eddies. These instabilities may have been generated by passing alongside the Phoenix High, causing division
365 into three smaller eddies (Fig. 7b). An analogy, albeit with much larger relief, may be found in the Lesser
366 Antilles; where large current eddies passing through gaps between the islands have been observed to break
367 up into a number of smaller "offspring" (Simmons and Nof 2001).

368 We speculate that the depth and prominence of the three troughs are due to the rotating eddies coming to a
369 relative halt close to the palaeo-self-slope break, possibly in response to a hydrographic boundary at this
370 point (e.g. Colling et al. 2001). Having come to a halt, the three eddies then dissipated their energy by drilling
371 down into the soft, unconsolidated substrate. Flow separation may have occurred at the edge of each
372 developing trough, with a zone of highly disturbed flow contained within a bubble. This would have led to
373 the current being directed downwards, with each vortex striking the surface at the reattachment point and
374 scouring the bed (Fig. 7b; Allen, 1994).

375 Having done their last work of erosion at the basinward end of each of the troughs, the rotating eddies could
376 then have either lost their power or alternatively “lifted off” from contact with the sea floor if, for example,
377 mixing with the surrounding water resulted in neutral buoyancy. This would explain the closed perimeter of
378 the depression, the position of the deepest erosional down-cutting features, and the inwards dipping
379 margins of the erosion surface. A similar phenomenon has been noted for the Mediterranean Outflow,
380 where a downslope bottom current is observed to “lift off” the sea floor at a critical depth in response to the
381 effects of relative buoyancy (Habgood et al. 2003).

382 It is notable, that for a south-east flowing current system, the erosional depression curves to the right, i.e. in
383 the opposite direction to the prevailing Coriolis Effect. However, a class of westward propagating mesoscale
384 eddies, rotating counter-clockwise in the southern hemisphere, has been observed on eastern ocean
385 boundaries (Miller et al. 2005). Hence, while overall motion seems to be in the “wrong” direction, internal
386 deflection is consistent with the Coriolis Effect. In the type area of the northwest Pacific, these are termed
387 Haida eddies, where they are observed to form at least once per year, with frequency rising in association
388 with El Nino events. The eddies are 150 to 300 km in diameter and travel at speeds up to 2 cm/s, though
389 internal rotation speeds of more than 30 cm/s, which are more than adequate to erode soft sediments, have
390 been observed (Miller et al. 2005). Vertical extent is typically up to 1,000 m (Di Lorenzo et al. 2005). Haida
391 eddies thus offer an analogue, albeit at a somewhat larger scale, for a bottom-impinging current system that
392 could have been responsible for erosion on the Walvis shelf.

393 In the southwest Atlantic, mesoscale clockwise eddies are postulated to act as a “submarine-polishing
394 machine” on the sea floor (Viana et al. 1998). In this mechanism, the vertical downwater transference of the
395 momentum generated by eddy rotation is strong enough to induce high bottom current velocities. These
396 then combine with upwelling Eckman pumping, which is characteristic for cyclonic eddies, to produce a
397 tornado-like effect along its core. In the northern South China Sea, Quaternary mesoscale eddies are
398 identified as erosional agents on the continental slope, albeit at a subtle level (Chen et al. 2019).

399 In the interpretation of the seismic stratigraphy, erosion and deposition are proposed to have taken place
400 concurrently, and this fits well within our proposed explanation of the erosional depression as having been
401 cut by bottom currents. The mutual interaction of erosional and depositional processes is indeed widely
402 observed in contourite systems (Rebesco et al. 2014), so accords well with our observations from the Walvis
403 shelf. We suggest that behind the erosive frontal edge of an active bottom current, the disturbed sediment
404 was being redeposited as downlapping clinoforms in its wake.

405 We postulate that the sequence of events occurred as follows:

- 406 1. Fine sediment re-suspended from the sea floor formed a benthic nepheloid layer. In deep water this
407 may be up to several hundred metres thick (Deuser et al. 1981).
- 408 2. Once out of the near bed region, sediment was held in suspension by the action of turbulence,
409 which, as well as being the agent of erosion, was responsible for most of the vertical transport within
410 the benthic boundary layer (Dade et al. 2001).
- 411 3. As the erosive eddies moved on and shear stress decreased below the settling threshold, suspended
412 sediment began to sink back from the nepheloid layer to the near bed region. This had the effect of
413 increasing the concentration of suspended sediment, thereby developing a density stratification,
414 which absorbed turbulent energy.
- 415 4. In turn, this reduced shear stress and facilitated deposition of the suspended load (McCave2004)
416 along clinoforms behind the advancing eddies, thereby preserving a local record of the direction of
417 movement.

418 In contrast, finer, slower settling particles were kept in suspension, even as shear stresses waned. In
419 particular, deposition of aggregates of diameter $<4\ \mu\text{m}$ may have been suppressed by relatively modest
420 current speeds (McCave 2004). Some of these finer particles then came under the influence of the deep
421 poleward current, and were transported to the south. The outcome was a fractionation process, in which
422 silts were preferentially deposited, and finer clays kept in suspension (McCave 2004) or transported away.
423 The initial infilling sediments are therefore predicted to be slightly coarser than their lateral neighbours in
424 the uneroded margins of the depression. This might be expected to result in a decrease in acoustic
425 impedance across the stratal discontinuity surface, and this would be consistent with the negative polarity of
426 the observed reflection.

427 **5.2 Significance of bottom current intensification at ca. 10 Ma**

428 A causal connection may plausibly be inferred between the intensification of the Benguela Current at ca. 10
429 Ma as identified from DSDP and ODP studies (Siesser 1980; Diester-Haass 1990) and the erosional and
430 depositional processes described in this paper. From their location, and from what is known of the palaeo-
431 circulation in the region, the water mass circulation responsible for the depression and its infill was most
432 likely to have been part of the BUS. What is less obvious is why these processes led to such profound
433 erosional sculpting at this particular time i.e. at ca. 9.9 Ma at this location. The Phoenix High was still present
434 as a sea floor swell, and the ABF is known to have moved up and down the coast in response to changes in
435 the BUS, so why has such an event not occurred more than once?

436 It is difficult to draw conclusions as to the precise combination of factors that led to such an extraordinary
437 erosional episode. However, it is interesting to speculate that it may have been that the initial intensification
438 in response to glacial activity in the Antarctic resulted in a “spike” in the intensity of the Benguela Current at
439 ca. 9.9 Ma. Subsequently, the levels of current intensity required to produce the forms observed, have not
440 been achieved since that time.

441 Another possibility is that relative sea level, which had been rising on the margin more or less steadily since
442 the Early Miocene (Siesser and Dingle 1981), reached a critical point over the study area at the same time as

443 the Benguela Current intensified. The suggestion here is that a particular “tuning” depth occurred at just the
444 right time, which enhanced the effects of eddy generation through the gap alongside the Phoenix High.
445 Whatever the direct cause, the effect was a massive excavation of near sea floor sediments in a large region
446 of the outer shelf, showing that the erosive effects of bottom currents can be intense, and highly focused,
447 and can leave a dramatic imprint in the stratigraphic record.

448 **6. Conclusions**

- 449 1. The erosional depression, including its sedimentary infill, records an episode of Late Miocene bottom
450 current intensification on the outer shelf of the Walvis Basin, and is a rare feature, with few if any obvious
451 analogues, either locally or globally.
- 452 2. On the basis of seismic to well ties, the basinward side of the erosion surface can be dated at 9.9 ± 1.0 Ma.
453 This constitutes a minimum age for the bottom current activity.
- 454 3. The depression coincides spatially with a low relief gap in sea floor topography next to the Phoenix High,
455 and with the approximate location of the ABF, and it is concurrent with the intensification of the BUS at ca.
456 10 Ma.
- 457 4. The relative importance of these factors, and of their coincidence, is unclear, though they are postulated
458 to have worked together in an unusual fashion to produce a “tuning” effect that resulted in the generation
459 of mesoscale eddies associated with bottom currents sweeping south-eastwards along the shelf, parallel to
460 the margin, and then turning sharply to the southwest into the basin.
- 461 5. The morphology of the erosion surface that defines the depression is closely related to the configuration
462 of the reflections from the sedimentary infill, and strongly suggests that deposition occurred in the wake of
463 the eroding eddies, and that erosion and deposition thus took place concurrently rather than sequentially.
- 464 6. The surface is thus interpreted to be diachronous, being younger at its basinward side.
- 465 7. The water depth at the time of formation of the depression was approximately 330 m.

466 In addition to these specific points, we draw the following general conclusions:

- 467 • Areally extensive erosion surfaces may be formed by bottom current activity on the continental
468 shelf, though instances are rare and depend on the convergence of a specific set of conditions.
- 469 • An erosion surface such as that studied in this paper may extend over an area much greater than
470 that covered by a typical 3D seismic survey. In such a case, incomplete coverage over an extensive
471 erosion surface may result in it being mistaken for a (regional) sequence boundary.

472 **Acknowledgements**

473 The authors are most grateful to NAMCOR, the National Petroleum Corporation of Namibia for granting
474 access to seismic and borehole data. Thanks are also due to Schlumberger for the donation of Geoframe
475 software and to IHS Markit for the donation of Kingdom software. The manuscript was greatly improved by
476 comments from an anonymous reviewer and from Roger Swart. The manuscript was greatly improved by
477 comments from an anonymous reviewer and from Roger Swart. AH was partly funded by the American
478 Association of Petroleum Geologists for work which included this study.

479 **References**

- 480 Abreu V, Sullivan M, Pirmez C, Mohrig D (2003) Lateral accretion packages (LAPs): An important reservoir
481 element in deep water sinuous channels. *Marine and Petroleum Geology* 20:631-648
- 482 Aizawa M, Bluck B, Cartwright J, Milner S, Swart R, Ward J (2000) Constraints on the geomorphological
483 evolution of Namibia from the offshore stratigraphic record. *Geol Surv Namibia Comm* 12:337-346
- 484 Allen J (1994) Fundamental properties of fluids, their relation to sediment transport processes In: Pye K (ed),
485 *Sediment Transport, Depositional Processes*. Blackwell Sci Publ Oxford 2:25-60
- 486 Ashcroft W (2011) *A Petroleum Geologist's Guide to Seismic Reflection*. Chichester, UK: John Wiley & Sons,
487 176pp

488 Bertoni C, Cartwright J (2006) Controls on the basinwide architecture of the Messinian evaporites on the
489 Levant margin, Eastern Mediterranean. *Sedimentary Geology* 188-189:93-114

490 Branney M (1995) Downsag, extension at calderas: New perspectives on collapse geometries from ice-melt,
491 mining, volcanic subsidence. *Bull Volcanol* 57:303–318

492 Brown L, Fisher W (1977) Seismic-Stratigraphic Interpretation of Depositional Systems: Examples from
493 Brazilian Rift and Pull-Apart Basins: Section 2 Application of Seismic Reflection Configuration to Stratigraphic
494 Interpretation. In: Payton (ed) *Seismic Stratigraphy-Applications to Hydrocarbon Exploration*, AAPG Memoir
495 26:213-248

496 Bull S, Cartwright J, Huuse, M (2009) A review of kinematic indicators from mass-transport complexes using
497 3D seismic data *Marine and Petroleum Geology* 26:1132-1151

498 Cartwright J, Santamarina, C (2015) Seismic characteristics of fluid escape pipes in sedimentary basins:
499 implications for pipe genesis *Marine and Petroleum Geology* 65:126-140

500 Catuneanu O (2003) *Sequence Stratigraphy of Clastic Systems*, Geological Association of Canada 16:1-248

501 Chen H, Zhang W, Xie X, Ren J (2019) Sediment dynamics driven by contour currents, mesoscale eddies
502 along continental slope: A case study of the northern South China Sea. *Marine Geology*, 409:48-66

503 Clement A, Gordon A (1995) The absolute velocity field of Agulhas eddies and the Benguela Current. *J*
504 *Geophys Res* 100 (CII):22,591-22,601

505 Colling A, Open University Course Team (2001) *Ocean Circulation*. Butterworth-Heinemann. 286pp

506 Corner B, Cartwright J, Swart R (2002) Volcanic passive margin of Namibia: A potential fields perspective In:
507 Menzies, M, et al (eds), *Volcanic Rifted margins*. *Geol Soc Am Spec Paper* 362:203-220

508 Dade W, Hogg A, Boudreau B (2001) Physics of flow above the sediment–water interface In: Boudreau, B,
509 Jorgensen, B (eds) *The Benthic Boundary Layer*. Oxford Univ Press New York 4-43

510 Deuser W, Ross E, Anderson R (1981) Seasonality in the supply of sediment to the deep Sargasso Sea,
511 implications for the rapid transfer of matter to the deep ocean. *Deep-Sea Research* 28:495–505

512 Di Lorenzo E, Foreman M, Crawford W (2005) Modelling the generation of Haida Eddies. *Deep Sea Research*
513 II 52:853-873

514 Diester-Haass L, Meyers P, Rothe P (1990) Miocene history of the Benguela Current and Antarctic ice
515 volumes; evidence from rhythmic sedimentation and current growth across the Walvis Ridge (Deep Sea
516 Drilling Project Sites 362, 532). *Paleoceanography* 5:685–707 doi.org/10.1029/PA005i005p00685

517 Emery D, Myers K (eds) (1996) *Sequence Stratigraphy*. Oxford. Blackwell Science. 297pp

518 Frey Martinez J, Cartwright J, Hall B (2005) 3D seismic interpretation of slump complexes: examples from the
519 continental margin of Israel. *Basin Research* 17.1:83-108

520 Fulthorpe C, Carter R (1991) Continental shelf progradation by sediment drift accretion. *Geol Soc Am Bull*
521 103.2:300–309

522 Garcia M, Hernández-Molina, F, Alonso B, Vázquez, J, Ercilla G, Llave E, Casas D (2016) Erosive sub-circular
523 depressions on the Guadalquivir Bank (Gulf of Cadiz): Interaction between bottom current, mass-wasting
524 and tectonic processes. *Marine Geology* 378:5-19

525 Gille S, Metzger E, Tokmakian R (2004) Seafloor topography and ocean circulation. *Oceanography* 17:47-54

526 Gornitz V (2009) Sea level change, post-glacial. In: Gornitz (ed) *Encyclopedia of Paleoclimatology and Ancient*
527 *Environments*. *Encyclopedia of Earth Sciences Series*. Springer:887-893

528 Green A (2009) Sediment dynamics on the narrow, canyon-incised and current-swept shelf of the northern
529 KwaZulu-Natal continental shelf, South Africa. *Geo-Mar Lett* 29:201-219

530 Habgood E, Kenyon N, Masson D, Akhmetzhanov A, Weaver P, Gardner J, Mulder T (2003) Deep-water
531 sediment wave fields, bottom current sand channels and gravity flow channel-lobe systems: Gulf of Cadiz, NE
532 Atlantic. *Sedimentology* 50:483-510

533 Hall S, Bird D, McLean D, Towle P, Grant J, Danque H (2018) New constraints on the age of the opening of the
534 South Atlantic basin. *Marine and Petroleum Geology* 95:50-66

535 Heine C, Zoethout J, Müller R (2013) Kinematics of the South Atlantic rift. *Solid Earth* 4:215-253

536 Holtar E, Forsberg A (2000) Postrift Development of the Walvis Basin, Namibia: Results from the Exploration
537 Campaign in Quadrant 1911. In: Mello M, Katz B (eds), *Petroleum Systems of South Atlantic Margins*. AAPG
538 Memoir 73 429-446

539 Huuse M, Lykke-Andersen H (2000) Overdeepened Quaternary valleys in the eastern Danish North Sea:
540 morphology and origin. *Quaternary Science Reviews* 19:1233-1253

541 Jackson M, Hudec M, Hegarty K (2005) The Great West African Tertiary coastal uplift: Fact or Fiction? A
542 perspective from the Angolan divergent margin. *Tectonics* 24:TC6014, doi:10.1029/2005TC001836

543 Jansen J, Ufkes E, Schneider R (1996) Late Quaternary Movements of the Angola-Benguela Front, SE Atlantic,
544 and Implications for Advection in the Equatorial Ocean. In: Wefer G, Berger W, Siedler G, Webb D (eds) *The*
545 *South Atlantic: Present and Past Circulation*. Springer-Verlag, Berlin Heidelberg 553-575

546 Lass H, Schmidt M, Mohrholz V, Nausch G (2000) Hydrographic and current measurements in the area of the
547 Angola-Benguela front. *Journal of Physical Oceanography* 30:2589-2609

548 Leeder M (1999) *Sedimentology, Sedimentary Basins: From Turbulence to Tectonics*. Blackwell Science,
549 Oxford 608pp

550 Light M, Maslanyj M, Greenwood R, Banks N (1993) Seismic sequence stratigraphy and tectonics offshore
551 Namibia. In: Williams G, Dobb A (eds) *Tectonics and Seismic Sequence Stratigraphy*. *Geol. Soc. Spec. Publ.*
552 71:163-191.

553 Masson D, Plets R, Huvenne V, Wynne R, Bett B (2010) Sedimentology and depositional history of Holocene
554 sandy contourites on the lower slope of the Faroe-Shetland Channel, northwest of the UK. *Marine Geology*
555 268:85-06

556 McCave I (2004) Size sorting during transport, deposition of fine sediments: sortable silt, flow speed In:
557 Rebesco, M, Camerlenghi, A (eds) *Contourites: Developments in Sedimentology* 60 Elsevier 121-142

558 McDonnell A, Loucks R, Dooley T (2007) Quantifying the origin and geometry of circular sag structures in
559 northern Fort Worth Basin, Texas: paleocave collapse, pull-apart fault systems, or hydrothermal alteration?
560 *AAPG Bulletin* 91.9:1295–1318

561 Miller L, Robert M, Crawford W (2005) Editorial: The large, westward-propagating Haida Eddies of the Pacific
562 eastern boundary *Deep Sea Res II* 52:845-851

563 Mitchum R, Vail P, Sangree J (1977) Seismic stratigraphy and global changes of sea level. Part 6, Stratigraphic
564 interpretation of seismic reflection patterns in depositional sequences. *AAPG Memoir* 26:117-133

565 Penduff T, Barnier B, Beranger K, Verron J (2001) Comparison of near-surface mean, eddy flows from two
566 numerical models of the South Atlantic Ocean *J Geophys Res* v106, C8, p16,857-16,867

567 Pérez-Díaz L, Eagles L (2014) Constraining South Atlantic growth with seafloor spreading data. *Tectonics*
568 33:1848–1873, doi:10.1002/2014TC003644

569 Posamentier H (2001) Lowstand alluvial bypass systems: Incised vs unincised *AAPG Bulletin*, v 85, No 10, pp
570 1771-1793

571 Pufahl P, Maslin M, Anderson L, Brüchert V, Jansen F, Lin H, Perez M, Vidal L, Shipboard Scientific Party
572 (1998) Lithostratigraphic summary for Leg 175: Angola-Benguela upwelling system In: Wefer, G, Berger W,
573 Richter C, et al *Proc ODP Init Repts 175: College Station TX (Ocean Drilling Program)* 533–542
574 [doi:10.2973/odp.proc.ir.175.118.1998](https://doi.org/10.2973/odp.proc.ir.175.118.1998)

575 Rebesco M, Hernandez-Molina F, Van Rooij D, Wahlin A (2014) Contourites, associated sediments controlled
576 by deep-water circulation processes: State-of-the-art, future Considerations, *Marine Geology* 352:111-154

577 Rommerskirchen F, Condon T, Mollenhauer G, Dupont L (2011) Miocene to Pliocene development of surface
578 and subsurface temperatures in the Benguela Current system. *Paleoceanography*, 26:PA3216
579 doi:10.1029/2010PA002074

580 Schumm S (1993) River response to base level change: Implications for sequence stratigraphy *Journal of*
581 *Geology* 101:279–294

582 Shannon L (1985) The Benguela ecosystem: Part I Evolution of the Benguela, physical features and processes.
583 *Oceanography and Marine Biology* 23:105–182

584 Sheriff R (1977) Limitations on resolution of seismic reflections and geologic detail derivable from them. In:
585 Payton, C (ed), *Seismic Stratigraphy - Applications to Hydrocarbon Exploration*. Memoir 26 AAPG Tulsa
586 Oklahoma 3-14

587 Siesser W (1980) Late Miocene origin of the Benguela upwelling system off northern Namibia. *Science*
588 208:283-285 doi: 10.1126/science.208.4441.283

589 Siesser W, Dingle R (1981) Tertiary Sea-Level Movements around Southern Africa. *J Geol* 89:83-96

590 Simmons H, Nof D (2001) The Squeezing of Eddies through Gaps. *J Phys Ocean* 32:314-335

591 Stewart S (2003) How will we recognize buried impact craters in terrestrial sedimentary basins? *Geology*
592 31:929-932

593 Stow D (1987) South Atlantic organic-rich sediments: facies, processes and environments of deposition. In:
594 Brooks J, Fleet A (eds) *Marine Petroleum Source Rocks*. *Geol Soc London Spec Publ* 26:287-299

595 Vail P, Mitchum R, Todd R, Widmier J, Thomson S, Sangree J, Bubba J, Hatleid W (1977) Seismic stratigraphy
596 and global changes of sea level. In: Payton, C (ed), *Seismic Stratigraphy - Applications to Hydrocarbon*
597 *Exploration*. Memoir 26 AAPG Tulsa Oklahoma 49-212

598 Verdicchio G, Trincardi F (2008) Mediterranean shelf-edge muddy contourites: examples from the Gela and
599 South Adriatic basins. *Geo-Mar Lett* 28:137–151

600 Viana A, Faugeres J, Kowsmann R, Lima J, Caddah L, Rizzo J (1998) Hydrology, morphology and
601 sedimentology of the Campos continental margin, offshore Brazil. *Sed Geol* 115:133-157

602 Van Andel T, Calvert S (1971) Evolution of sediment wedge, Walvis shelf, southwest Africa. *J Geol* 79:585-602

603 Ward J, Corbett I (1990) Towards an age for the Namib. In: Seely, M (ed), Namib ecology: 25 years of Namib
604 research Transvaal Museum Monograph 7, Pretoria 17–26

605 Wefer G, Berger W, Richter C, et al. (eds) (1998) Proc ODP, Initial Reports, 175 Ocean Drilling Program,
606 College Station, Texas [doi:10.2973/odp.proc.ir.175.1998](https://doi.org/10.2973/odp.proc.ir.175.1998)

607 Weigelt E, Uenzelmann-Neben G (2004) Sediment deposits in the Cape Basin: Indications for shifting ocean
608 currents? AAPG Bull 88.6:765–780

609 Wonham J, Jayr S, Mougamba R, Chuilon P (2000) 3D sedimentary evolution of a canyon fill (Lower Miocene-
610 age) from the Mandorve Formation, offshore Gabon. Mar Petrol Geol 17:175–197

611 **Figure Captions**

612 **Fig. 1** Regional setting showing the Benguela Upwelling System in the Cape Basin: South Atlantic Current
613 (SAC), Current Benguela Coastal Current (BCC), Benguela Oceanic Current (BOC), Angola Current (AC) and
614 Angola-Benguela Front (ABF – along-coast movement shown by the black two-headed arrow). After Jansen
615 et al. 1996. *P* marks the site of the buried Phoenix volcano (Corner et al. 2002)

616 **Fig. 2** Base map for seismic profiles and boreholes. The area covered by Fig. 3 and the location of Fig 4 are
617 also shown

618 **Fig. 3** Two-way travel time contour map of the erosion surface and the surrounding correlative conformity
619 surface (contour interval = 0.025 s (25 ms)), with locations of Figs 5, 6, 8 and 10

620 **Fig. 4** Regional seismic profile (dip orientation) showing the major post-rift tectono-stratigraphic units of the
621 Walvis Basin. The erosional surface that forms the depression is evident immediately below the seabed
622 reflection at the top right of the Fig. See Fig. 2 for location

623 **Fig. 5** Representative strike (a) and dip (b) oriented profiles across the erosional depression. Intersection
624 shown as dashed red line. Horizons shown are: Near Top Palaeocene (orange); Near Top Eocene (red); Near

625 Top Early Miocene (magenta); Late Miocene erosional surface (yellow); top of lower infilling unit M1 (green).
626 Examples of key reflection characteristics are highlighted. See Fig. 3 for locations

627 **Fig. 6** Seismic profiles across deep pits, A, B and C in strike orientation (a) and dip orientation (b), (c) and (d);
628 intersections marked with red dashed vertical lines. Faults omitted for clarity. Horizons shown are: Near Top
629 Early Miocene (magenta); Late Miocene erosional surface (yellow); top of lower infilling unit M1 (green).
630 Examples of key reflection characteristics are highlighted. See Fig. 3 for locations

631 **Fig. 7** a) Three-dimensional rendering of erosional depression and surrounding correlative conformity
632 surface. Horizontal axes: 120 x 80 km; vertical axis: 1.2 seconds TWTT; b) Close-up 3D view of erosional
633 depression looking to the NNE showing the suggested path of erosive eddies. Red arrows indicate
634 intensification of erosion and direction of subsequent downlapping sedimentation around outer edge

635 **Fig. 8** Seismic profile across the buried Turonian-Cenomanian Phoenix volcanic edifice (*P*). Horizons shown
636 are: Base Cenozoic (beige); Near Top Palaeocene (orange); Near Top Eocene (red); Near Top Early Miocene
637 (magenta); Late Miocene erosional surface (yellow); top of lower infilling unit (green). Note the influence
638 that Phoenix continues to exert on present-day sea bed topography, and the location of the erosional
639 depression with respect to the sea floor bulge. See Fig. 3 for locations

640 **Fig. 9** Example of shelf delta, approximately 150 km along the shelf to the southeast of the study area, used
641 to estimate palaeo-water depth

642 **Fig. 10** Seismic profile intersecting ODP borehole 1080A showing the hole terminating above the correlative
643 conformity of the erosion surface (yellow). Also shown is the Near Top Early Miocene horizon (magenta).
644 Stratigraphic tops are from Wefer et al. (1998). See Footnote for information on time-depth conversion. See
645 Fig. 3 for location

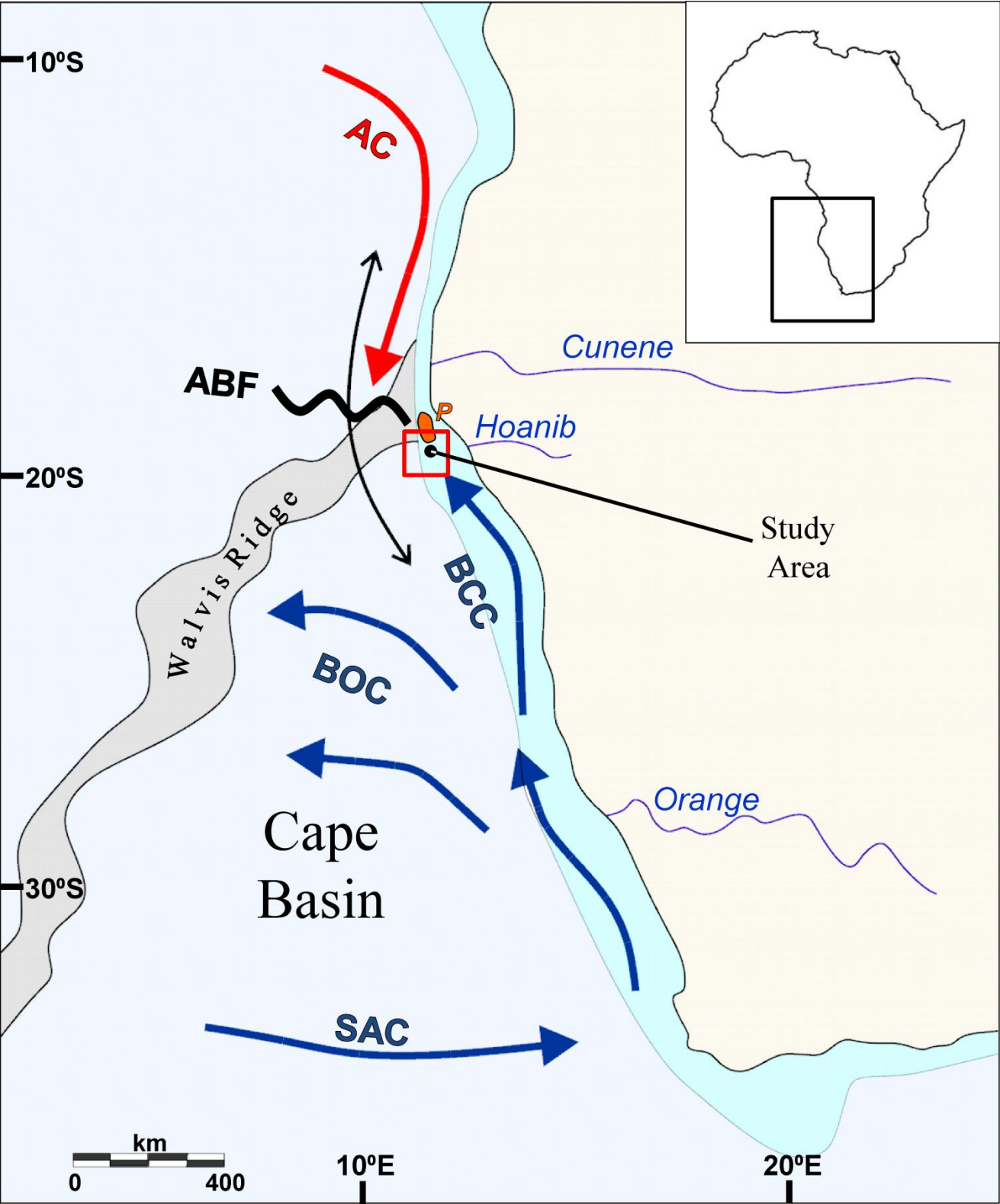


Figure 1

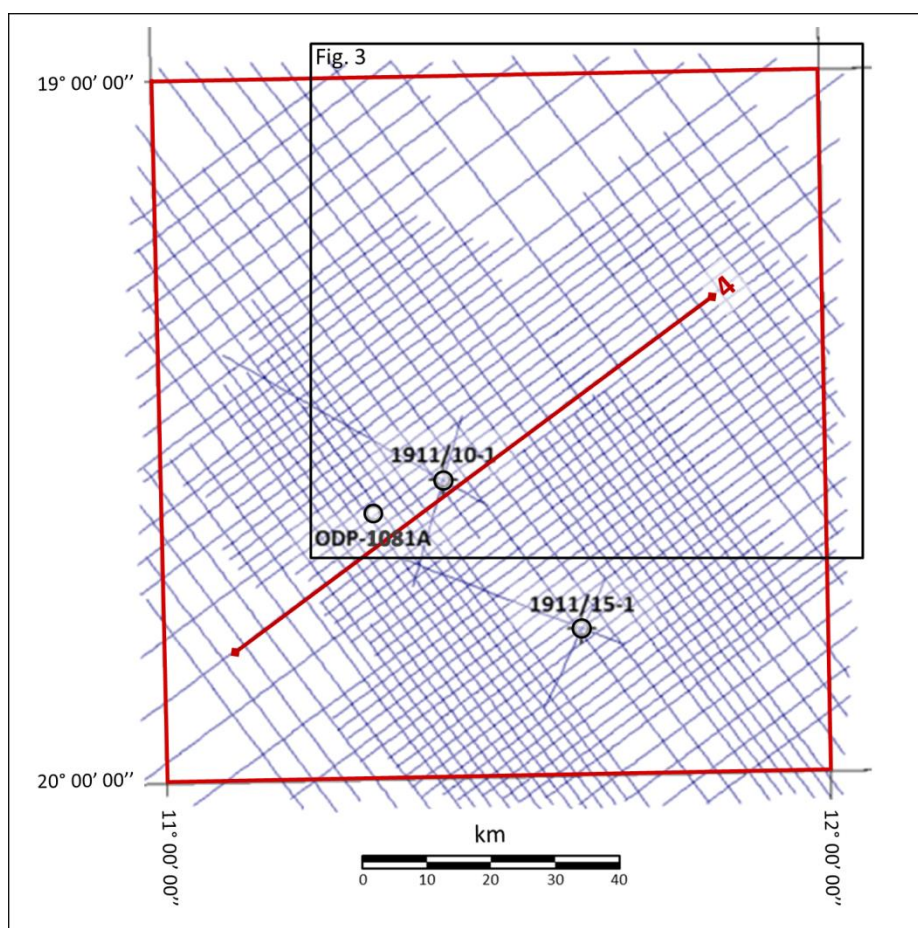


Figure 2

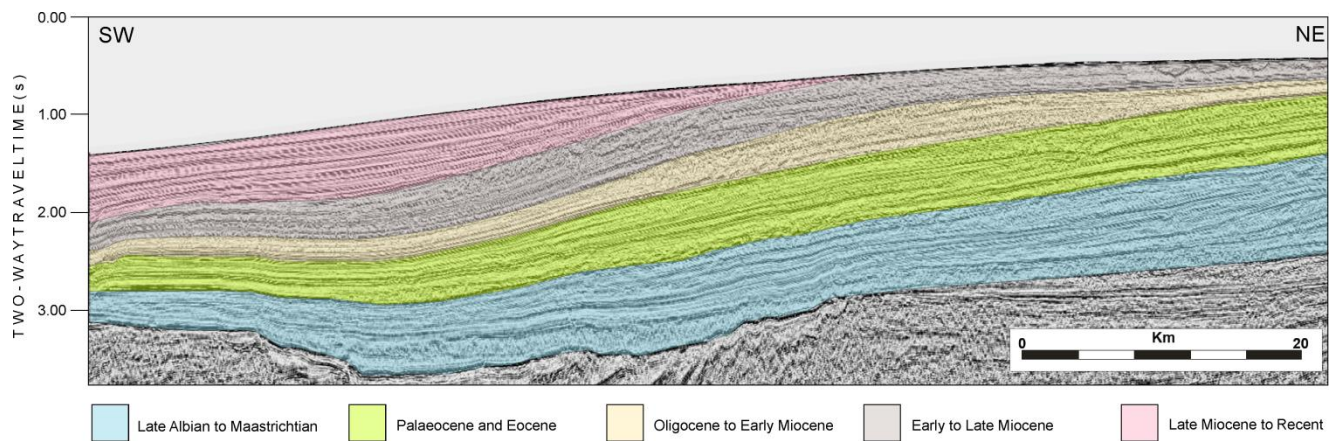


Figure 4

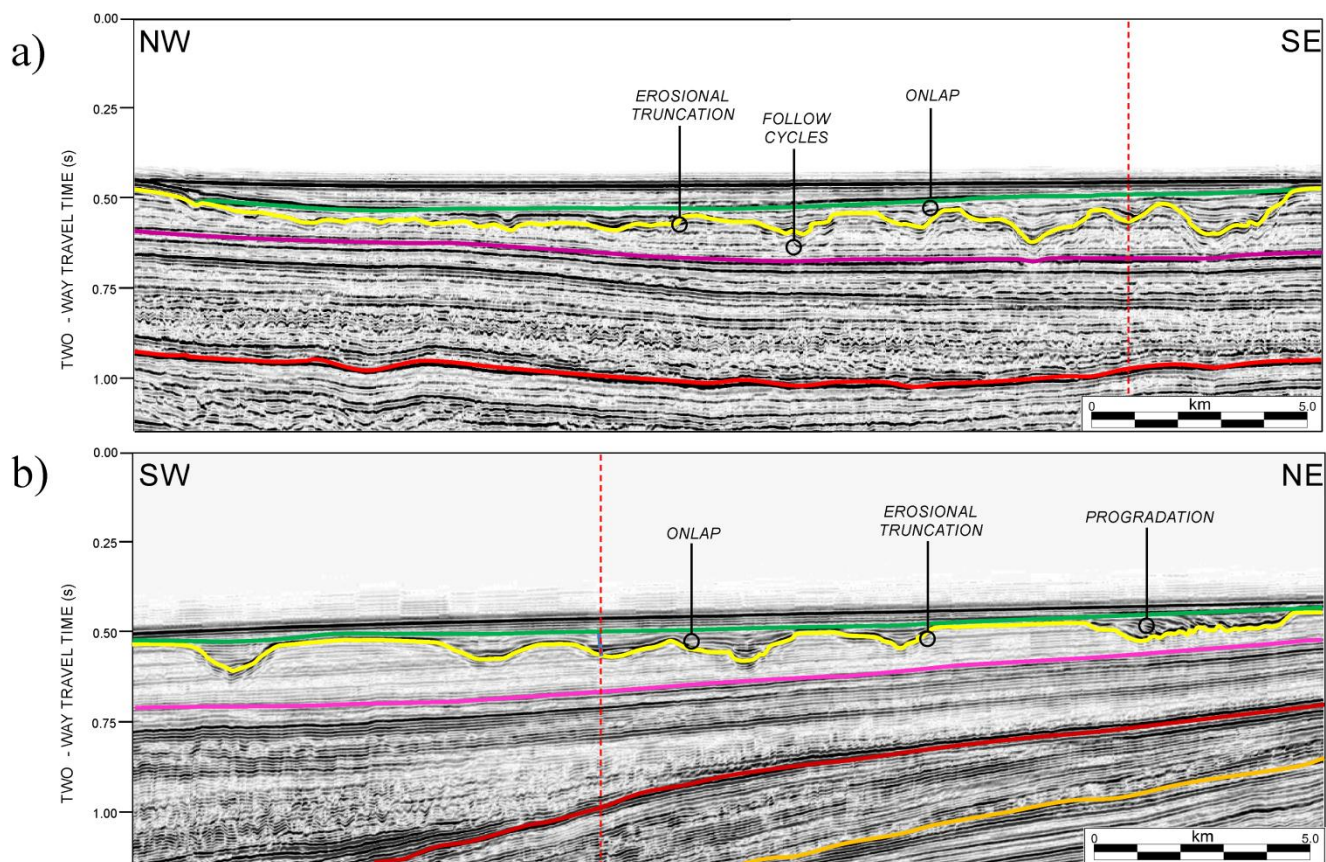


Figure 5

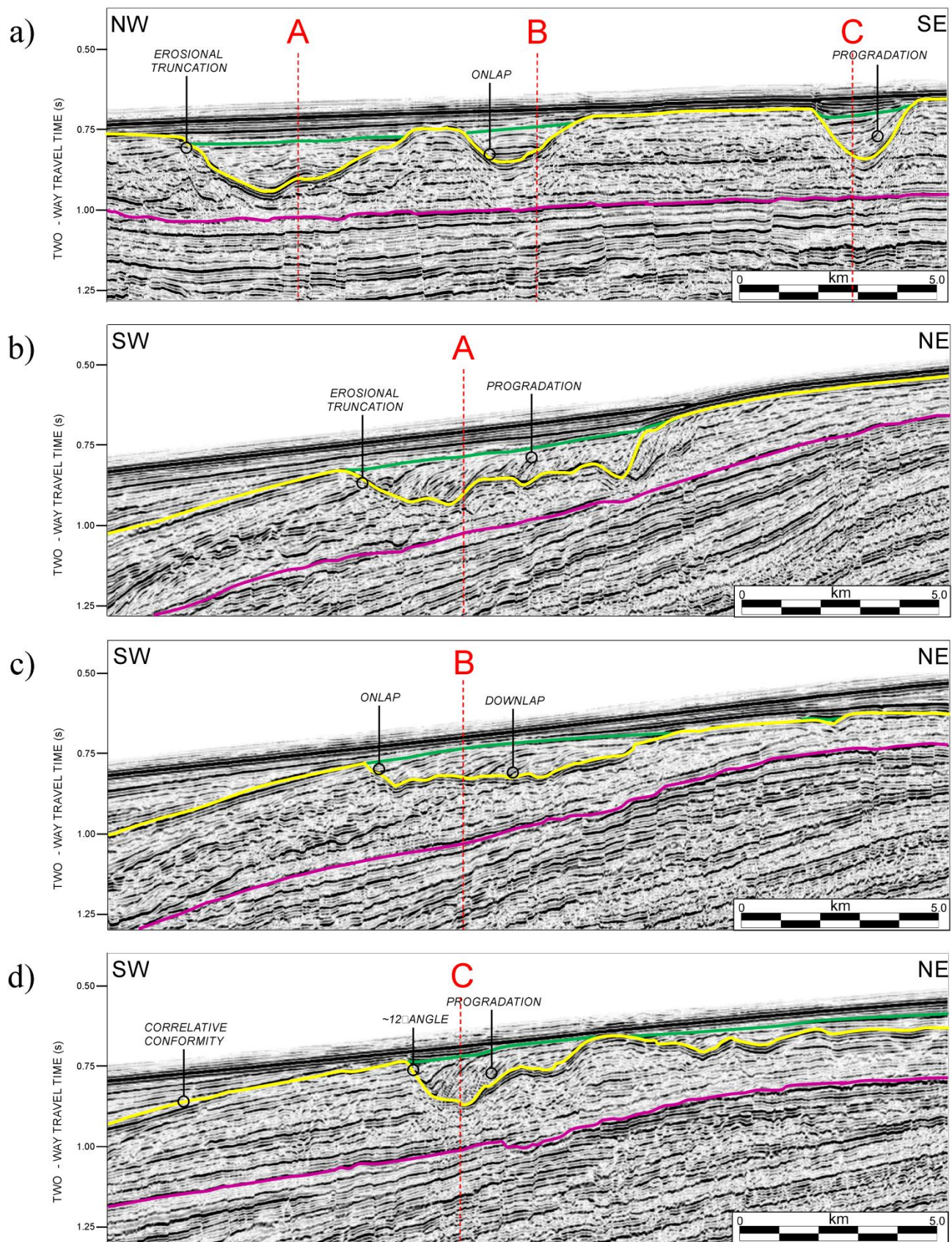


Figure 6

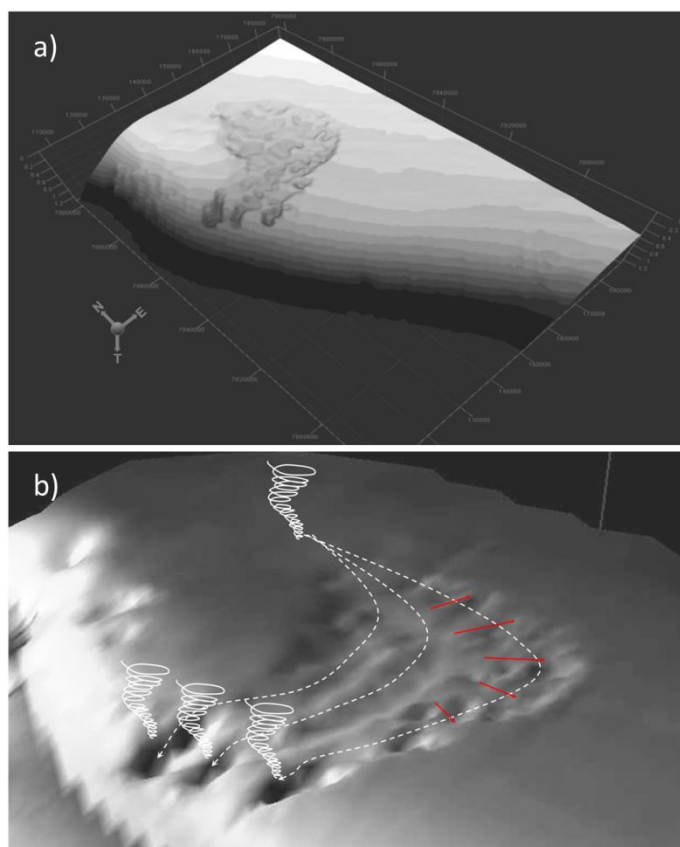


Figure 7

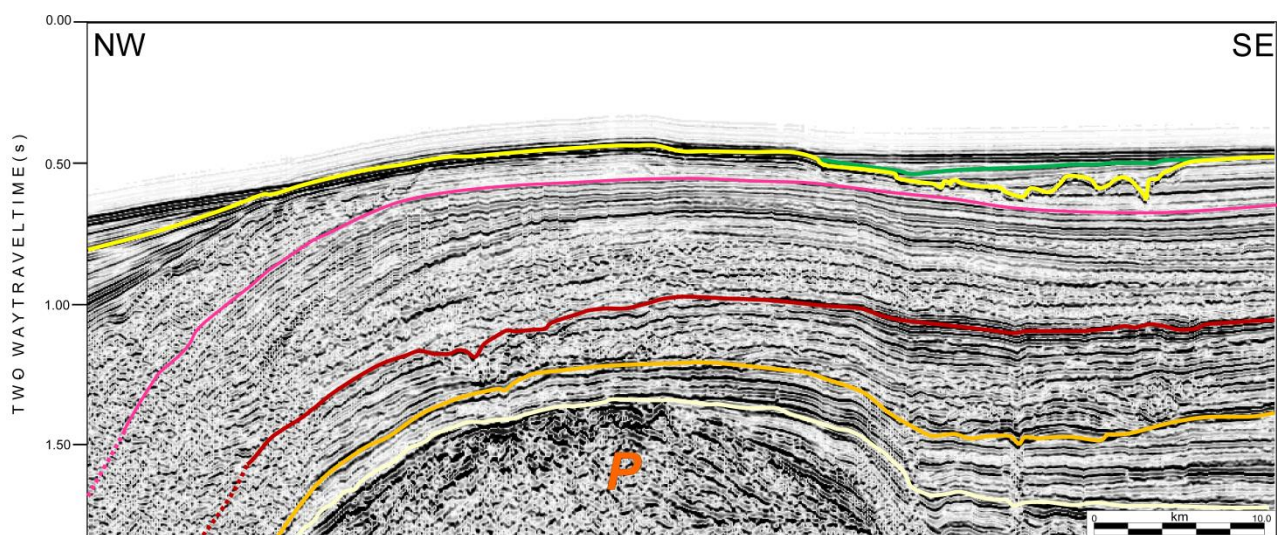


Figure 8

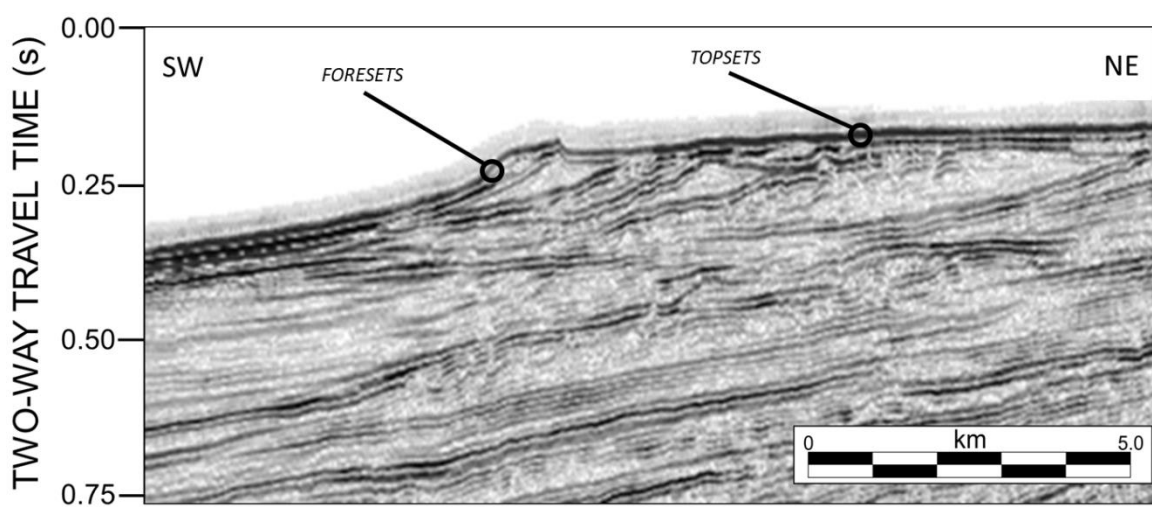


Figure 9

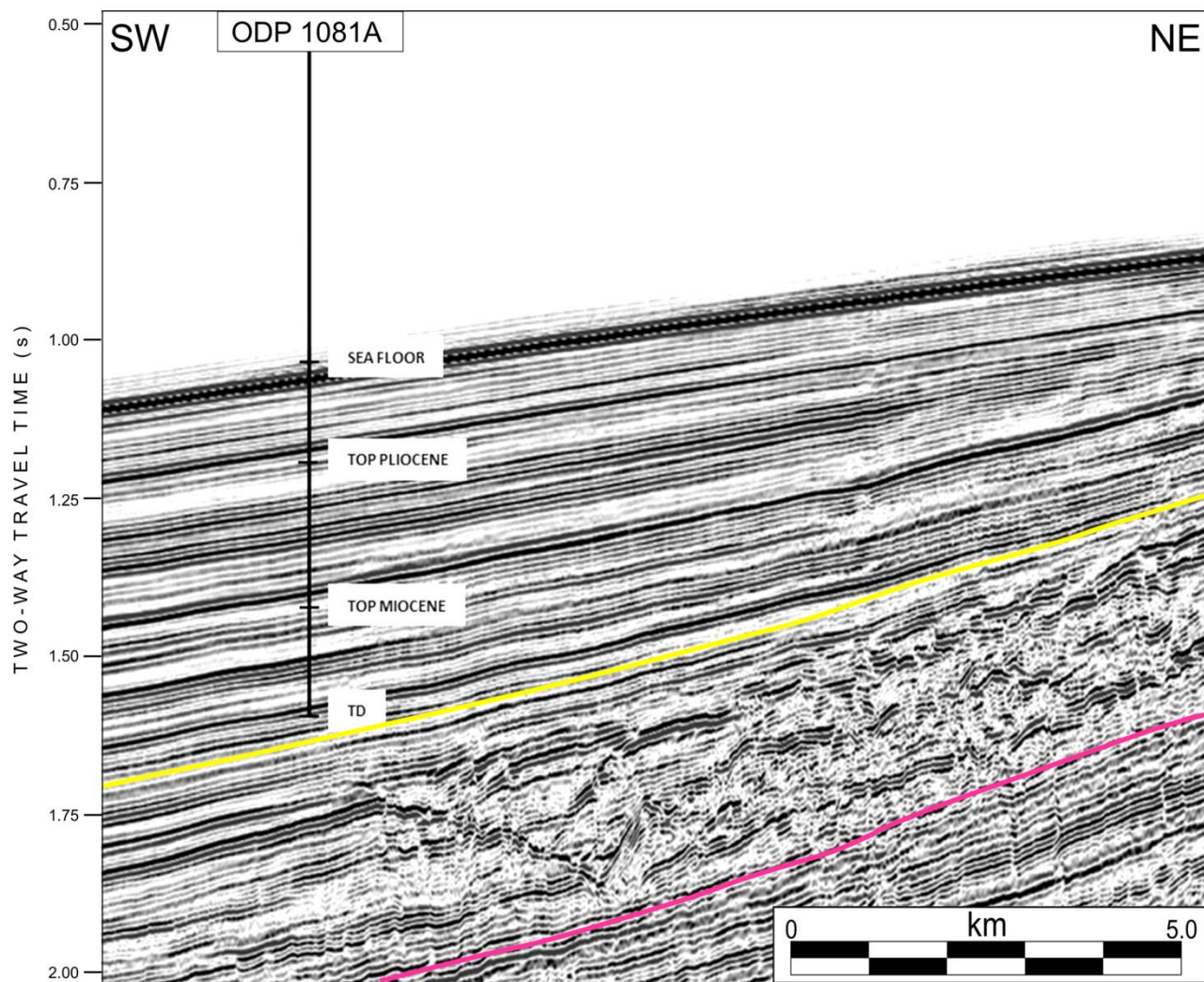


Figure 10